Radar Based Human Vital Sign Detection In Cars
A System Analysis

by

Roeland Kooij
Saliha Neji

Electrical Engineering Bachelor Final Project
Faculty of Electrical Engineering, Mathematics and Computer Science
Delft University of Technology

Student names:	R. Kooij (4313801)	S. Neji (4606795)
Thesis committee:	Prof. Dr. A. Yarovoy	
	Dr. F. Fioranelli	
	Dr. J. C. Varon Perez	
Coordinator:	Dr. Ir. I. E. Lager	
Supervisor:	Dr. F. Fioranelli	
Project duration:	April 20, 2020	June 30, 2020

An electronic version of this thesis is available at `http://repository.tudelft.nl/`.

TUDelft

Abstract

This thesis analyses different radar systems for sensing chest movement to detect human presence inside a car. The detection in this thesis is limited to sensing breathing rate, although heartbeat detection is considered a possibility. A comparison is made between CW-, FMCW-, pulsed- and UWB pulsed radar. UWB pulsed radar was chosen to be a suitable technology for this application. As a benchmark, the Xethru X4 SoC by Novelda is used. The parameters and the working of Xethru X4 are investigated. A suitable antenna for Xethru is designed and simulated. Different detection techniques are discussed. The feasibility of the Xethru X4 is tested by means of calculations in different settings. Based on these tests, the Xethru X4 is evaluated on concluded to be suitable for detecting human presence inside a car by means of vital sign detection.

Contents

1

Introduction

1.1. Problem Description

When the summer comes the intense heat from the sun can raise a car's interior temperature to very dangerous levels. According to KidsAndCars.org, every year on average 39 babies die in hot cars due to heatstroke [1]. In nearly all of these cases the deaths happen accidentally and could have been prevented. To prevent such accidents a detector for human presence is needed. This thesis will explore a radar system that senses human vital signs to detect human presence. This system can be deployed to prevent 'baby in hot car' deaths but could also be deployed for other purposes such as non-contact human vital sign monitoring in a hospital or nursery home setting.

The vital signs that are of interest in this system are breathing rate and heart rate. The detection of humans can be divided into different levels of detail:

- Binary presence of a human.

- Monitoring breathing rate and heart rate over time.

- Concluding physical conditions of a human using breathing- and heart rate data.

Binary presence detection uses radar data to find breathing and/or heartbeat patterns to identify human presence. For monitoring, accurate detection of every single breath and heartbeat is required for satisfying results. To derive physical conditions, algorithms are needed that use monitored breathing- and heart rates. The scope of this thesis is limited to binary presence detection. For the context of preventing heatstroke deaths in cars, this is all the information that is needed.

For the application of the radar system, the device will be placed inside a vehicle. As mentioned before, the goal is to detect humans inside the vehicle. The exact location of these targets is not important for the context at hand. The device has to detect chest movement at breathing- and heartbeat frequencies.

To approach this problem a list of goals and challenges is comprised:

- Identifying different radar techniques and finding a suitable fit for the application of in-car use.

- Exploring relevant radar system parameters and set a list of requirements for the application of in-car use.

- Modelling the target and environment, in this case a moving human chest and a car interior respectively.

- Designing a theoretical prototype based on a combination of products on the market, simulated devices and theoretical devices.

- Analyse a system based on the Xethru X4 System on Chip radar

1.2. Thesis Synopsis

This thesis presents a system analysis on a radar system for detecting human vital signs in a car. Chapter 2 contains the requirements relevant to the application. Chapter 3 contains a comparison of different radar systems and presents a radar type suitable for for the application. Chapter 4 gives a detailed description of all the relevant components and parameters present in an UWB radar, outlining the basis for the design of a Xethru X4 based radar system. In chapter 5 an antenna is designed and simulated and a radar system is modelled to simulate how it will operate in the given application. Chapter 6 discusses the design approach and results from these simulations. In chapter 7 a conclusion is presented based on the requirements and the system analysis.

2

Program of Requirements

In chapter 1 the problem of sensing human vital signs for human presence detection has been introduced. The solution for this problem is restricted by a set of user requirements. This chapter will define these requirements and consider different sensing technologies that can fulfil the requirements.

2.1. User Requirements

The problem defined in chapter 1 has to be solved in an indoor car environment. In this context a list of requirements can be defined to make the system realistic and feasible. These requirements are listed below:

1. The system must be able to detect any human presence inside a vehicle.

2. The system needs to be able to detect human presence within a 1 minute time frame.

3. The system needs to be able to detect human presence based on human vital signs.

4. The system needs to be small, low profile, and thus non-intrusive inside the car environment.

5. The system needs to be non-intrusive and non-contact with the car's passengers.

6. The system must be fully operational automatically whenever the car is parked, for at least 2 hours.

7. The detection range of the system should cover the entirety of a standard family vehicle.

8. Detection should be possible in cluttered and reflective environments.

9. Humans that are hidden from the system by car seats, clothes, blankets, etc. should still be detectable.

2.2. State-of-the-Art Analysis

To fulfil the listed user requirements, several non-contact detection technologies were identified. All of the identified technologies have potential to detect human presence through vital signs detection, each with their respective advantages and disadvantages. This thesis will analyze the most viable technology for human vital sign detection.

2.2.1. Acoustic Sensing

Acoustic sensing uses information contained in sound waves to detect human vital signs. A method for detecting heartbeat and breathing rate is by listening to the sound that is produced by these motions. This can be achieved using a passive sensing system using microphones [2]. The detection can also be done actively, using a sonar device [3]. This technology tends to be inaccurate at range and is best deployed in contact applications. Acoustic sensing suffers severely from environmental noise, which can be tens of decibels stronger than the signal at range.

2.2.2. Camera Sensing

This is a type of passive sensing, where ambient light is reflected from a human target and captured by a RGB-thermal camera. The camera senses tiny changes in the skin color to detect bloodflow and thus heart rate. A thermal camera captures changes in the skin temperature around the nose to detect breathing rates [4]. This technology is able to detect human vital signs but suffers from many disadvantages. First of all, the camera system is generally expensive and the signal processing is tasked with large amounts of data. In the context of a hot car environment, the thermal imaging of the breathing rate would become difficult due to large amounts of ambient infrared light. The technology will also not work in conditions with poor visibility or when trying to detect non-line-of-sight targets.

2.2.3. LIDAR

Light detection and ranging is another type of optical sensor that uses an active transmission of light for detection. Because the transmitter and receiver are time synchronised, this type of system can determine range. This technology suffers from the same disadvantages as a camera based system, where the detection is difficult or even impossible in low visibility conditions and when targets are hidden out of sight.

2.2.4. RADAR

Radio detection and ranging (Radar) is an active sensor that sends radio waves at targets and receives the reflections using antennas. Because radar systems use electromagnetic waves, it is possible to penetrate materials and identify targets in non-line-of-sight conditions. In the context of detecting passengers inside a vehicle, this is a very big advantage, since targets are often hidden behind obstacles such as car seats, blankets and clothes. Conducting materials such as metal, are impenetrable for radio waves. Since cars are essentially big metal boxes, a radar system deployed inside a car will be mostly isolated from the outside environment. When the car environment is subjected to high temperatures, the radar detection will not suffer in principle. Human vital sign detection using radars has become common among researchers [5–7].

2.3. System Requirements

In this thesis the viability of radar technology will be tested by means of a system analysis. There are many different ways to implement radar technology, these options are explained in chapter 3. Which type of radar is best suited for human presence detection inside a vehicle depends on a list of system requirements. These requirements are listed below and are based on the user requirements listed in section 2.1.

1. The radar system needs to be a single device that is small and can be mounted inside a car in a non-intrusive way.

2. The accurate detection range of the radar needs to be at least 4m, to account for the longest possible path from the radar towards a target inside a vehicle (depending on where the radar is mounted, this value can be less)

3. The transmitter and receiver antennas should have a wide beam width to cover all possible angles at which targets can be located inside the vehicle. A narrow beam would require mechanical scanning or phased array scanning which is not feasible for the application.

4. The radar's operating frequency should be chosen such that penetration of expected obstructions inside a car is possible

5. The radiated power at the transmitter must not exceed safety regulations

6. The receiver should provide a signal for processing with a Signal to Noise Ratio (SNR) of at least 3dB.

7. The system should be fitted with a backup battery for power when the car is parked.

These specifications form a baseline for the system design. In the next chapter, different radar technologies are discussed and based on the system requirements, a radar system will be chosen for in-car human vital sign detection. In chapter 4 these requirements are translated into numerical parameters.

<div style="text-align: right; font-size: 3em;">3</div>

Radar Techniques

This chapter identifies different radar techniques and explains how they achieve target detection. Different techniques have different advantages and disadvantages. Using the user- and system requirements from chapter 2, an optimal system is chosen for human vital sign detection inside a car.

3.1. Continuous Wave (CW) Radar

Continuous Wave (CW) radar is a basic form of radar. It operates with a wave signal that is continuously broadcast on an antenna. Objects in the environment will reflect this signal into a receiver, which can detect this wave signal by scanning a range around the broadcasted frequency. The signal can have its frequency shifted by objects moving radially with respect to the radar causing a Doppler shift. This frequency shift is useful for determining the velocity of detected objects. When the transmitter and receiver are located at the same position and the velocity of moving objects is many times smaller than the speed of light, the observed Doppler frequency f_d can be calculated using the following equation [8]

$$f_d = \frac{2 v_r f_c}{c} cos\theta_{cone} \qquad \text{[Hz]} \quad (3.1)$$

where v_r is the velocity relative to the radial axis from the radar, f_c is the transmitted signal frequency, c is the speed of light and $cos\theta_{cone}$ is the cone angle which can be expressed as $cos\theta_{cone} = cos\theta cos\phi$, where θ and ϕ are respectively the azimuth and the elevation of the target as seen by the observer. The Doppler effect illustrates how CW radar can be used to determine the velocity of moving objects. Such Doppler radars are used for example in radar guns to measure the speed of vehicles on the road, but can also be used for detecting small movements such as human vital signs [7, 9].

3.2. Frequency Modulated Continuous Wave (FMCW) Radar

The possibilities of CW radar can be extended by modulating the wave signal. A common method is frequency modulation, where the carrier frequency is changing over time. The most used modulation signal is a sawtooth signal. This signal sweeps the carrier frequency from a low value to a high value repeatedly. By using such a modulation a time signature is added to the signal. At the receiver, the time signature of the transmitted signal and received signal can be compared to calculate the round trip time, and thus the range. Using the roundtrip time t_r and the speed of light c, the perceived range R to the target is defined by:

$$R = \frac{c * t_r}{2} \qquad \text{[m]} \quad (3.2)$$

3.3. Pulse Doppler Radar

The pulse Doppler radar works by transmitting a pulse then receiving the reflected pulse. The pulses have a certain width and are transmitted with pulse repetition frequency (PRF). The PRF determines the maximum unambiguous range that can be detected. The relation between the maximum unambiguous

range and the PRF is as follows:

$$R_{max} = c \frac{T_{PRI}}{2} = c \frac{1}{2 f_{PRF}} \qquad \text{[m]} \quad (3.3)$$

where c is the speed of light, T_{PRI} is the pulse repetition interval and f_{PRF} is the pulse repetition frequency. The signal spectrum of a pulse radar is a combed line spectrum. The spacing between the lines is equal to the PRF and determines the velocity's unambiguity, since the maximum unambiguous Doppler shift is

$$f_{d,max} = \frac{f_{PRF}}{2} \qquad \text{[Hz]} \quad (3.4)$$

When a Doppler shift occurs, the received spectrum is shifted with respect to the transmitted spectrum. If the Doppler frequency exceeds the PRF/2, the velocity measurement becomes ambiguous. This is where the Doppler dilemma arises, since a high PRF is needed for large unambiguous velocity, but a low PRF is needed for large unambigous range [10]. PRF will therefore vary depending on the context at hand.

3.4. UWB Pulsed Radar

A radar system with a bandwidth exceeding 500MHz or 20% of the center frequency is considered an Ultra-Wideband (UWB) radar. The essentials of a pulse radar system described in the previous section still apply to UWB radars, however there are some added advantages when using UWB. UWB radars typically use a time dependant modulation on the transmitted pulses. This modulation spreads the spectrum of the transmitted signal but also adds a time signature to the pulse. Range resolution for normal pulse radars is determined by the pulse width. If a pulse is 50cm wide and it hits two targets, separated by 10cm, then the echoed pulses of both targets will overlap and the targets can not be distinguished. Using pulse modulation and spreading the bandwidth, this resolution is greatly increased. For UWB radars with pulse modulation, the smallest distinguishable range between targets is dependant on the transmitted bandwidth B and is defined by the following formula:

$$S_r \geq \frac{c}{2B} = \frac{c\tau}{2} \qquad \text{[m]} \quad (3.5)$$

where τ is the pulse width.

3.5. Suitable Radar for Vital Sign Detection

To be able to detect human vital signs, a radar has to be able to either detect chest displacement or velocity. To measure chest displacement the time varying target range is analyzed to extract breathing and heartbeat frequencies. To measure chest velocity, the doppler shifted frequency of the reflected signal is compared with the transmitted signal. Two radar detection techniques for vital sign detection can be identified which have their respective optimal radar system:

- Vital sign detection using time-varying range.

- Vital sign detection using Doppler shift.

3.5.1. Vital Sign Detection using Time-Varying Range

Movement of the heart and lungs translates into chest expansive and contractive motion. Breathing induces a peak expansion of the chest of around 2cm when viewed from the front (along the antero-posterior axis) at a frequency of around 0.2Hz [11]. A radar aimed at a human chest will perceive a time-dependant range to the target that contain the breathing and heartbeat frequency. By accumulating range data from the receiver, using signal processing these frequencies can be extracted. Chest movement due to heartbeat will be much smaller in comparison to breath movement, therefore this thesis will focus on breathing detection as a proof of concept.

To detect human vital signs using range, a high range resolution is desired. As was discussed in section 3.4, UWB radar takes advantage of pulse modulation while using a large bandwidth to achieve very high range resolution. An example of an UWB radar system that is used for vital sign detection is the Novelda Xethru X4 [12]. This System on Chip (SoC) radar operates at a center frequency of 7.29GHz with a 1.5GHz bandwidth. With these parameters, and using equation 3.5 the range resolution

is calculated at 10cm. For indoor applications, which in the context of this thesis is inside a car, a 10cm range resolution, which is high in terms of radar parameters, is desirable as it allows a better distinction between targets of interest and clutter.

3.5.2. Vital Sign Detection using Doppler Shift

Another approach for detecting chest movement is by looking at the Doppler-shift at the receiver. The velocity of chest movement is perceived at the receiver by means of a shifted frequency in comparison with the reference transmission signal. When using the chest movement parameters presented in section 3.5.1 and assuming a sinusoidal periodic chest movement, the peak velocity will be about 0.013 m/s. Using formula 3.1 the expected doppler shift can be calculated. If for example a 6GHz center frequency is used for detection, the received signal will be shifted by 0.5Hz during peak velocity of the chest. This is a very small amount of doppler shift, and is therefore hard to distinct from stationary clutter in a short amount of time. Additionally, this doppler shift measurement is subject to phase noise, which is explained in section 4.5.2.

3.5.3. Choice of Radar System

Now that different radar techniques and detection techniques are identified, a radar system can be chosen for vital sign detection inside a car. To make this choice, first a brief comparison is made between the introduced techniques in table 3.1. Using the advantages and disadvantages in combination

Table 3.1: Radar Comparison

Radar Technique	Advantages	Disadvantages
CW	- Continuous sensing - Low peak power - Simple hardware	- No range detection
FMCW	- Detects range+velocity - Low peak power	- Increased complexity compared to CW - Non-linearity in modulation
Pulsed Radar	- Detects range+velocity - High SNR	- Trade-off range and velocity resolution - High peak power
UWB pulsed radar	- High range resolution - Less subject to outside interference	- Trade-off range and velocity resolution - High peak power

with the requirements from chapter 2, UWB pulsed radar was chosen to be a suitable radar technique for vital sign detection inside a car. The biggest benefit is the high range resolution, which in indoor applications, where environmental signal reflections are prominent, is a very big advantage.

3.5.4. Novelda Xethru X4 UWB pulsed radar

An example of an UWB pulse radar for vital sign detection in indoor applications is the Xethru X4 by Novelda. This radar, shown in figure 3.1, is built as a System on Chip (SoC) using CMOS technology [12]. The viability of this radar will be tested in this thesis using theoretical arguments and simulations. In the next chapter, a system analysis of an UWB pulsed radar system will be done, taking the most relevant parameters into the context of our application, and justifying the Xethru X4 as a viable option. The overview of the circuit is given in the appendix A.1.

Figure 3.1: Novelda Xethru X4 SoC UWB radar

4

UWB Pulsed Radar System Analysis

This chapter will explain in detail the design of an UWB pulsed radar. First, a block diagram of the system is given, showing relevant components of the radar device as well as relevant environmental features.

4.1. Block Diagram

The block diagram of the radar system is given below. The diagram is based on the Xethru X4 infrastructure. The sections in the rest of this chapter will reference these blocks and explain how they contribute to the system.
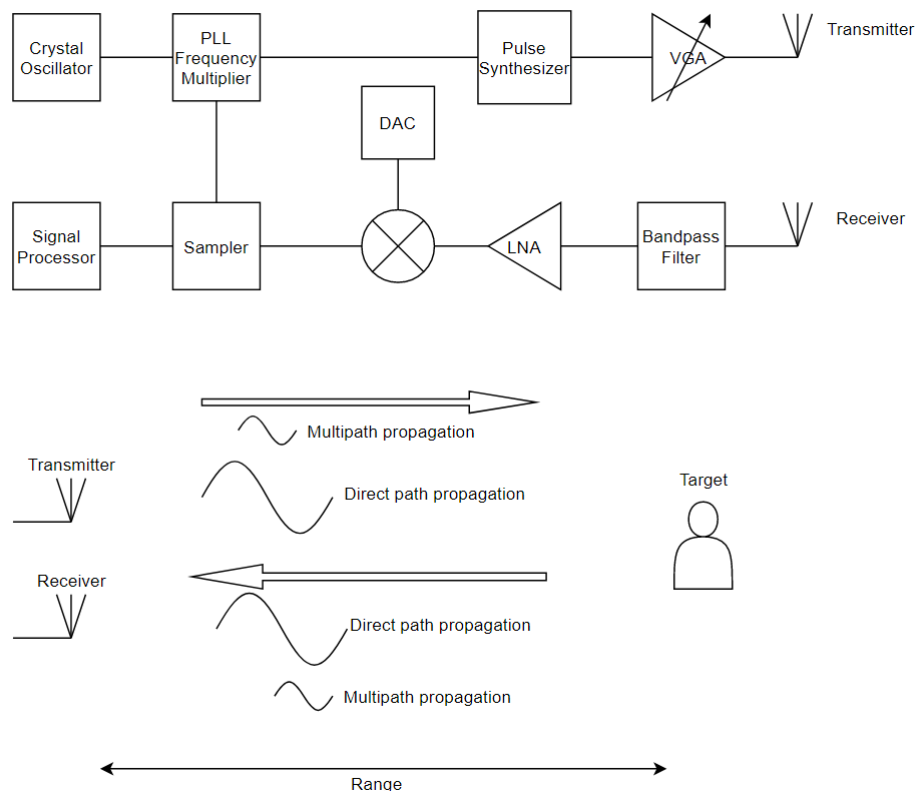

Figure 4.1: Block diagram of the radar system (top) and the environment (bottom)

9

4.2. Waveform

An UWB pulsed radar sends pulses of a carrier signal into the environment. There are several parameters that determine the shape and characteristics of this waveform. In figure 4.2 a simple representation of a pulsed radar signal is given. The pulses have pulse width τ and the number of pulses transmitted in 1 second is given by the pulse repetition frequency (PRF). The frequency of the carrier signal f_c is also the center frequency of the pulsed signal bandwidth. The bandwidth B of the transmitted is signal is inversely proportional to the pulse width τ. This relation is given in equation 4.1.

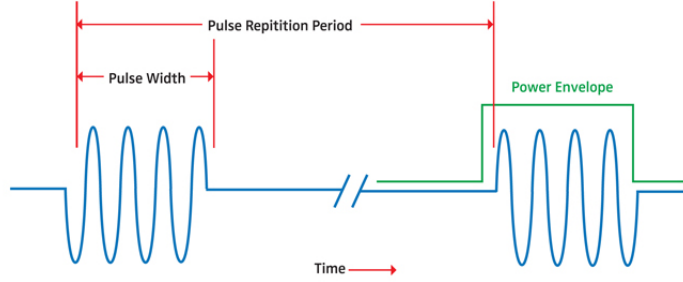$$B = \frac{1}{\tau} \qquad \text{[Hz]} \quad (4.1)$$

Figure 4.2: Signal waveform of a pulsed radar [13]

Modulation techniques can be employed such that the relation 4.1 does not remain valid. This is more discussed in 4.2.2.

4.2.1. Carrier Frequency

The carrier frequency determines the center position of the bandwidth. By using a higher carrier frequency, all of the transmitted frequencies are shifted into the higher frequency spectrum. Propagation properties are also frequency dependant, low frequency EM waves penetrate further into materials while higher frequency waves are more easily attenuated [10]. When using a radar inside a car, the EM waves have to be able to penetrate car seats and fabrics without losing much energy to detect humans. Signal frequency will also affect the physical size for a suitable antenna. This is explained in more detail in section 4.4.

The carrier frequency for radar systems is commonly generated by a crystal oscillator, shown in figure 4.1. The crystal oscillator should be stable enough to ensure low phase noise for accurate Doppler shift detection. This is more discussed in 4.5.3.

As has been explained in section 3.1, the carrier frequency influences the amount of Doppler frequency shift perceived in baseband according to the formula 3.1. Therefore, it can be adjusted such that the range-Doppler dilemma can be minimized. The maximum unambiguous range, given in formula 3.3, and maximum unambiguous Doppler shift, given in 3.4, can be combined together to obtain the total range-Doppler coverage

$$R_{max} f_{d,max} = \frac{c}{2 f_{PRF}} f_{PRF} = \frac{c}{2}$$

Substituting 3.1 and taking $cos\theta_{cone} = 1$ yields the range-velocity coverage

$$R_{max} v_{max} = \frac{c^2}{4 f_t} \qquad (4.2)$$

This means that to improve the range-velocity coverage, the carrier frequency should be increased to very high values which is unfeasible. Therefore, a choice has to be made between range or Doppler shift detection and thus the carrier frequency has to be chosen based on Doppler shift detection.

Relation 4.2 shows that the range-Doppler coverage is independent of the PRF frequency i.e. there is no optimum PRF at which both Doppler shift and range can be reliably detected.

4.2.2. Xethru X4 waveform

The Xethru X4 uses a signal with a center frequency of 7.29 GHz and a bandwidth of 1.4 GHz. At this frequency the Xethru X4 operates around the border between the radar C- and X bands, and is approved worldwide for unlicensed indoor use since the occupied bandwidth falls within limits defined by the FCC (US), ETSI (Europe) and KCC (Korea). The signal waveform is similar to the signal depicted in figure 4.2 however, the Xethru X4 uses a binary phase shift keying (BPSK) modulation on the carrier signal within a pulse to further spread the spectrum of the signal, increasing the bandwidth [12]. This spectrum spreading happens in the pulse synthesizer shown in figure 4.1. In the same figure a Phase Locked Loop (PLL) frequency multiplier can be seen. A PLL is a negative feedback loop that stabilises at the input frequency. By adding a multiplier or a decimator in the loop, integer fractions of the input frequency can be generated with very high stability. How a PLL works is described in detail in section 4.6.4. In the Xethru X4 the PLL scales the oscillator frequency by 5x to the desired 7.29 GHz carrier frequency.

A big advantage in using a high carrier frequency is the consequent ability to use very small antennas, which is explained in section 4.4.

4.3. Transmitted Power

Signal transmission can be done at different power levels. As has been stated in chapter 2, the radiated power must not exceed safety margins or spectral regulations. The FCC defines the emission limits by power spectral density (PSD) in dBm/MHz. For UWB in the range of 3.1 - 10.6 GHz, this limit is -41.3 dBm/MHz. The Xethru X4, with a 1.4 GHz bandwidth is therefore limited to -9.9 dBm average emitted power. The X4 data sheet lists 3 peak power settings of -0.7, 4.1 and 6.3 dBm [12]. The average power however is determined by the ratio between the pulse width and the pulse repetition period, also known as the duty cycle. These parameters can be set to different values, the settings are listed in the data sheet [12]. Using maximum power settings, the average power does not exceed -9.9 dBm as can be seen in table 4.1. Calculations can be found in the Matlab code in appendix B.1.

$P_{peak}[dBm]$	$E_{pulse}[pJ]$	$\tau[ns]$	$P_{avg,max}[dBm]$
-0.7	0.45	0.52	-17.39
4.1	1.47	0.57	-12.25
6.3	2.65	0.62	-9.69

Table 4.1: Power ratings of Xethru. $P_{avg,max}$ is calculated at the maximum $prf = 40.5 MHz$.

4.4. Antenna

For signal transmission and receiving, an antenna is needed. UWB Radar systems are typically monostatic, which means the transmitter and receiver are very close to each other and thus co-located. In some systems the transmitter and receiver share the same antenna [14].

4.4.1. Radiation

Antennas radiate EM waves when an alternating voltage causes charges in the antenna to accelerate periodically. The EM field produced becomes disconnected from the antenna and is radiated into the environment. Every antenna has a certain EM radiation pattern, which shows the antenna gain in dBi (gain in dB relative to an isotropic antenna which radiates uniformly in all directions). This pattern reveals hot spots and dead spots of the radiation. This information is important when considering antenna placement. Antennas for long range applications are generally highly directive, focusing most of the radiated power into a small beam. For short range, indoor applications, a wide radiation pattern is desirable. This eliminates the need for mechanical scanning to detect targets at a large variety of angles.

When designing an antenna for a certain application this is where a trade off has to be made between coverage and signal gain. If the energy input to the antenna is to remain constant, and the coverage is increased to twice the area, then the signal gain in that area is halved (-3dB). In practice, antenna's do not have a perfect beam; the gain is highest in a certain direction and gradually reduces when deviating from this hot spot. The beam width is commonly defined as the range of angles where the signal gain

is within -3dB with respect to the highest gain in the radiation pattern.

4.4.2. Bandwidth

Antenna designs for UWB applications come in a variety of shapes and sizes and are generally more complex than narrowband antenna's. Antenna designs such as a simple halfwave dipole are very resonant at a certain frequency. At this frequency the antenna radiates very efficiently, however frequencies around the resonance are mostly reflected back into the radar system.

If we model an antenna as a 2-port, the S_{11} parameter defines the reflected signal energy at the input of the antenna. S_{11} is expressed in -dB which relates the amount of reflected signal energy proportional to the total input signal energy. The antenna bandwidth is commonly defined as the range of frequencies where the S_{11} lies below -10dB. This definition can be changed depending on the radar application. For low powered radar systems such as an indoor UWB radar, a -10dB return loss is acceptable and will thus be used to define antenna bandwidth. UWB antennas deploy techniques that introduce multiple resonances at a range of frequencies to reduce wideband return loss [15].

4.4.3. Antenna for in-car UWB radar

The antenna used for human vital sign detection inside a car has to be compliant with the requirements from section 2. The most important requirements for antenna design are that the system must be small and low profile, and that the system's detection must cover the entire car. These requirements ask for a small antenna with a low directivity.

Antenna size is linearly inversely proportional to the operating frequency, a halfwave dipole for example is the size of half the signal wavelength. High frequencies have short wavelengths and are radiated by short antennas. For UWB radar in the GHz range it is common to use patch antennas [16–18]. These antennas are flat and can be implemented on a printed circuit board (PCB). In certain applications, high directivity is desired. For this purpose a phased array configuration of patch antennas can be used to get high directivity in a variable direction. This configuration deploys an array of antennas operating at different phases to form amplified modes in the radiation pattern. The modes can be steered by controlling the phase of each patch in the array. This technique can be used for detecting human vital signs with low power consumption and low clutter interference but comes with the disadvantage of increased system complexity [19]. This complexity is beyond the scope of this thesis, therefore a radar system will be considered with one transmitter antenna and one receiver antenna. In section 5.1 a design of a microstrip patch antenna suitable for the Xethru X4 is simulated.

4.5. Information Acquisition

Information about the velocity of the chest movement due to respiration can be obtained by either detecting the change of range over time or detecting Doppler shift induced by the chest movement. Both means are discussed in this section and the most suitable is selected for vital sign detection of infants in cars.

For a complex sinusoidal the transmitted signal expressed as follows

$$x(t) = A\cos(2\pi f_c t + \theta) = Re\left\{\left(Ae^{j\theta}\right)e^{j2\pi f_c t}\right\} \qquad \frac{-\tau}{2} \leq t \leq \frac{\tau}{2} \quad (4.3)$$

where f_c is the carrier and θ being the phase. As the signal propagates, the amplitude will be modified to $\tilde{A}$ due to losses which include free space loss, atmospheric losses .. etc. Furthermore, the received signal will be delayed with time duration that is

$$y(t) = x\left(t - \frac{2R}{c}\right)$$

Substituting yields

$$y(t) = \tilde{A}\cos\left(2\pi f_c\left(t - \frac{2R}{c}\right) + \theta\right) = \tilde{A}\cos\left(2\pi f_c t - \left(\frac{4\pi R}{\lambda}\right) + \theta\right) \qquad (4.4)$$

This applies for a stationary target. When the target is in motion, the sampled received signal can be modeled as follows [20]:

$$y[n] = \tilde{A}exp\left\{j\left[2\pi\left(\frac{2v}{\lambda}\right)nT + \theta - \left(\frac{4\pi R}{\lambda}\right)\right]\right\} \qquad 0 \leq n \leq N - 1 \quad (4.5)$$

where T is the pulse repetition interval in $[s]$ and the sample frequency being at least equal to the inverse of the pulse width such that the range can be measured at sample n.

The formula 4.5 shows that the Doppler information is contained in the phase of the received signal. Furthermore, the delay of the received signal is proportional to the range. This model is used to explain detection methods and the non-idealities that can compromise the measurement.

4.5.1. Displacement

Since the transmitted EM waves travel at the speed of light, the range can be detected by calculating the travel time where $R = 0.5ct_{prop}$. This can be done by sampling the received signal after a pulse is transmitted. If a signal is detected, then the time instant at which this signal is detected is the sample index multiplied by PRI. This means that the sampling frequency should be at least equal to the transmitter's bandwidth to ensure that a pulse fits in a single sample, otherwise aliasing will occur. Therefore, the range can be calculated by $R = 0.5cnPRI$. The change in the detected range yields the velocity.

In addition, the received signal will be delayed with $2R/c$ with respect to the transmitted signal and the phase will be shifted with $4\pi R/\lambda$ as shown in the formula 4.4. Therefore, a coherent detector can be used to obtain range information in the phase.

4.5.2. Doppler shift

Detecting Doppler shift can be done by phase measurement of the received signal as the received signal will have a phase shift proportional to the Doppler shift as shown in formula 4.5. The phase detection is done using a coherent detector, so that phase information is preserved. Coherent detectors are more deeply discussed in 4.6.3. Signal processing is performed in order to obtain the frequency of the Doppler shift. This can be done using FFT of the received signal which shows the Doppler shift of the target.

4.5.3. Phase noise and Clutter

Phase noise arises from instability of the frequency in the local oscillator in the transmitter. This instability causes the wave to have slightly different phases around the carrier frequency at different time instants. The change in phase is random. The oscillator's signal is used as a reference signal in the coherent detector. After transmitting a pulse with a certain phase shift, if the phase shift of the oscillator at the detector does not remain the same at the moment of detection, then phase noise will occur. This compromises the accuracy of the detected information. Since reflected signal from stationary objects (clutter) do not have phase shift and their spectrum should be at 0 Hz, distinction between moving and stationary reflections can be made. However, due to phase noise, clutter can have a slight phase which leads to their spectrum being around 0 Hz instead of exactly at 0 Hz. Movements that have low Doppler shifts are most subjected to this problem. Low pass filtering in this case will not work because the clutter might interfere with the Doppler shift of interest. The distinction between stationary and slowly moving objects is no longer clear. Specialized signal processing techniques can be employed to overcome the clutter problem such that Doppler shift can be distinguished.

4.5.4. Multipath Propagation

The radar system will be used inside a car. Except for the windows, a car is essentially a metal box. EM waves at UWB frequency in the C- and X-band are reflected by metals and can not be penetrated. This phenomenon causes the waves radiated from a radar system to reach the target not only through a direct path, but also via reflections in the environment. This is called multipath propagation and depending on the context and application can lead to very big problems in target detection. Figure 4.3 shows how multipath propagation leads to paths of different length between the radar and the target. Assuming the target is always in line of sight of a direct path, the multipaths will always be longer. A problem arises when the radar receives multiple signals from different paths and the signals overlap. As has been discussed in section 3.4, the ghost targets seen by longer reflected paths can not be distinguished when the signals overlap. For this reason it is essential that the radar has a good range resolution, described in formula 3.5. When the range resolution is in the centimeter range, ghost target seen by multipath propagation will be seen separately by the receiver. This makes UWB radars very robust against multipath fading [21].
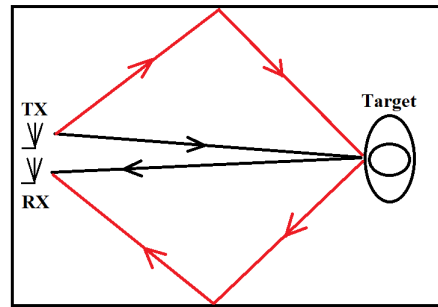
Figure 4.3: A radar and a target located inside a reflective environment, showing direct propagation in black and multipath propagation in red.

In the context of vital sign detection, the periodic change in range is the interesting variable, the absolute range to the target is not important. With good range resolution, the real target, as well as the ghost targets will all be seen oscillating at chest motion frequencies. This allows the radar to have more information on the target by capturing much more signal energy. Regardless of multipath, absolute range detection should still be possible using an algorithm in signal processing that detects ranges where human vital sign oscillation can be seen. By identifying the shortest range where this occurs, the direct path is derived, since it is always the shortest path.

4.6. Signal Detection

Many detection methods can be employed to obtain velocity information of the chest movement. This section discusses the possible methods and determines the most suitable method for vital sign detection of infants in cars.

4.6.1. Low Noise Amplifier (LNA)

When the signal is captured by the receiver it is very weak. Additionally the signal contains noise of all frequencies. Thus the signal can be band-pass filtered to only include frequencies corresponding to the signal bandwidth. This improves the SNR. Before detection can be done on the signal it has to be amplified first. This is done by a low noise amplifier (LNA) as can be seen in figure 4.1. A typical LNA can achieve a gain of 20 dB while only degrading the SNR by less than 3dB.

4.6.2. Swept Threshold Sampling

The Xethru X4 uses swept threshold sampling to convert the received signal from analog to digital (ADC). Instead of using N bit quantizers at different thresholds, it uses single 1 bit quantizer. To still retrieve all the information with a single quantizer, the input signal is biased with a sweep signal. This can be seen in figure 4.1 where a DAC produces a sweep signal, which is mixed with the received signal. The signal bias level is swept while the quantization threshold is fixed, however depending on the point of reference, it can also be interpreted as an untouched signal with a swept threshold. Using this technique a very high resolution is achieved with just a 1 bit quantizer. The output of the quantizer is sampled at 23.328 GS/s generating a digital reproduction of the pass-band signal.

4.6.3. Coherent I/Q detector

Coherent detector yields information about the phase of the received signal which can be employed in many radar technologies and not only pulsed radar. A block diagram of the coherent I/Q detector is shown in figure 4.4. This can be used for Doppler and range detection. The received signal is mixed with the reference signal, which is the transmitter's oscillator. To detect the in-phase and quadrature components of the signal, the received signal is split in 2. Each signal is connected to a mixer that is connected to the reference. The reference signal is shifted 90 degrees in one mixer with respect to the other. Effectively, the received signal is multiplied with the reference. Since the received signal is sinusoidal, the multiplication with another sinusoidal signal will yield 2 sinusoidal signals, one with the

phases added together and the other subtracted, according to the geometric relation:

$$2cos(a)cos(b) = cos(a - b) + cos(a + b)$$

$$2cos(a)sin(b) = sin(a + b) - sin(a - b)$$

This allows the detection of the cos component of the received signal i.e. the in-phase or I component and the shifted reference allows the detection of the sin component of the received signal i.e. the quadrature or Q component. The terms that correspond to the subtraction of the phases are captured for further processing, because the information lies in the difference between the reference phase before and after transmission. The terms that correspond to the addition of the phases are discarded by means of a low pass filter, since those terms have higher frequency.
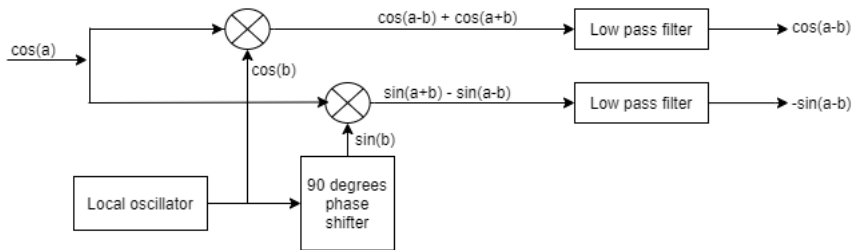

Figure 4.4: Block diagram of coherent I/Q detector.

Although common in many radars, the Xethru X4 does not use analog I/Q detection. Instead it uses CMOS technology for digital signal processing in a CPU micro controller using sampled data, see figure 4.1.

4.6.4. Phase-locked Loop (PLL)

A diagram of PLL is shown in figure 4.5. The main use of the PLL in Xethru is to change the frequency of a signal. The output signal will have a frequency that is equal to the input frequency multiplied by the frequency division factor N.
The PLL consists of phase comparator, low pass filter and voltage controlled oscillator (VCO). The phase of the input signal is detected with a coherent detector with the VCO signal being the reference. The low pass filter is applied to discard the term with the phases added together. The VCO then generates a signal with the new phase. The output of the VCO is then fed back to the phase comparator at which the input signal is compared with the VCO again. By adding a frequency divider in the loop, the VCO output frequency will stabilize at the inverse factor and will thus be multiplied to a multiple of the frequency input to the PLL.
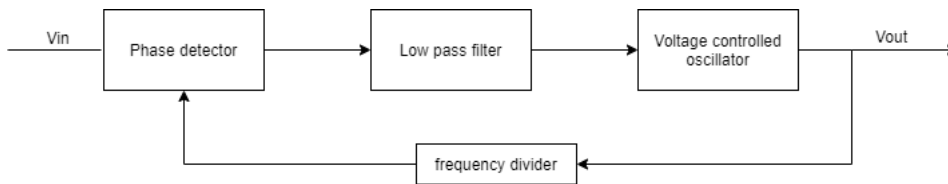

Figure 4.5: Block diagram of phase-locked loop.

4.6.5. Threshold detection

The threshold can be determined such that the receiver makes the distinction between reflected pulses and noise. This is done on the fast time data. The output can be characterized as binary 1 for detection event. Consequently, the magnitude information is lost. For range detection, the required information is the sample index at which the decision is true, therefore, the magnitude information can be discarded.
It is required to have a minimized threshold, such that detection can occur even with reflected signals that have low power. Ideally, the threshold should be the minimum received power from the reflections. However, this is highly effected by th noise. Therefore, the SNR of the system determines the minimum required threshold for reliable detection.

Keeping the threshold minimized is characterized by high probability of detection P_D. At the same time, the threshold should be high enough such that noise will not be detected. This is characterized by low probability of false alarm P_{fa}. Increasing the threshold will cause both probabilities to increase which leads to a trade off between P_D and P_{fa}. Therefore, a trade off should be made when determining the detection threshold. As a consequence, one variable can be examined in terms of the other two variables. This is done in section 5.5.

4.6.6. Coherent and noncoherent integration
Multiple pulses can be transmitted during a single measurement. The received pulses can be processed either coherently or noncoherently. Coherent integration is simply adding the received complex signals i.e phase and magnitude. If the target is in motion, then the received phases will be different such that they can either add up or cancel out depending on the value. Coherent integration a suitable detection method for Doppler shift, since Doppler shift detection is done by detecting the phase of the reflected signal.

Coherent integration also improves the SNR. If the minimum required SNR is calculated based on noise estimation at a single pulse, which can be randomly high, it causes a redundant high SNR value. Integrating over a number of pulses allows to average the noise on those pulses and thus the SNR will be improved by amount equal to the number of integrated pulses $SNR_{coh} = N_{pulses}SNR$ [22].

As for noncoherent integration, only the magnitudes of the reflected pulses are integrated, therefore, phase information is lost. As a consequence Doppler shift cannot be detected, however, range can still be detected by means other than phase detection. The SNR improvement of noncoherent integrator is less than the improvement of coherent integrator [22]. The integration is not linearly performed, therefore the noncoherent integration gain is always less than the number of pulses.

The Xethru X4 uses coherent integration of the pulses which allows for Doppler shift detection and improved SNR.

4.6.7. Radar Equation
The received power can be calculated from the radar equation as follows:

$$P_r = \frac{P_t G_{ant}^2 \lambda^2 \sigma}{(4\pi)^3 R^4} \qquad \text{[W]} \quad (4.6)$$

where P_t is the power of the transmitted signal, λ is the wavelength which is equal to c/f_c where c is the speed of light and f_c is the carrier frequency, σ is the radar cross section in m^2, $R^4 = R_t^2 R_r^2$ is the range of the target in m and $G_{ant} = G_{tx}G_{rx}$ the gain of the transmitter and receiver antenna. For monostatic radars $R_t = R_r$ and $G_{tx} = G_{rx}$ (refer to section 4.4). The noise power at the receiver is as follows:

$$P_n = kTFB \qquad \text{[W]} \quad (4.7)$$

where k is Boltzmann's constant, T is the reference temperature in Kelvin, F is receiver's noise figure and B is the bandwidth of the receiver in Hz. The SNR is therefore

$$SNR = \frac{P_r}{P_n} = \frac{P_t G_{ant}^2 \lambda^2 \sigma}{(4\pi)^3 R^4 kTFBL} \qquad \text{[-]} \quad (4.8)$$

The SNR can change depending on techniques used in the radar system. For coherent integration, a gain of N_{pulses} can be achieved. In addition, pulse compression yields a gain of $N_{PC} = B\tau$ [23] which is already included in the peak power as given in the datasheet [12]. Furthermore, a loss of L can be modeled due to system losses which is assumed to be around $1dB$.

The calculation is done in MATLAB, the code is given in appendix B.1 and the results are shown and discussed in section 5.4.

In addition, the car's environment suffers from high temperatures in the summer when left under the sunlight. The temperature can rise up to 45 degrees Celsius when left for one hour in the sun [24]. This has implication on the SNR since it is inversely proportional to the temperature. While Xethru promises to operate in temperatures between -40 to $+80$ degrees Celsius, the noise at the receiver will be changed. This is demonstrated with calculations in section 5.3.

4.7. System Power Supply

In chapter 2 it was mentioned that the system should operate on battery power when the car is parked. To implement this requirement for a Xethru X4 based system, a lithium battery with a USB charging controller can be used. This technology is widely used in portable devices such as smartphones. Cars of today's generation are almost all fitted with USB outputs, which allows for easy installation of the system.

5

UWB Pulsed Radar Modeling

In this chapter a simulation of an UWB pulsed radar is done based on the parameters from the Xethru X4 SoC UWB pulsed radar produced by Novelda. First, an antenna is designed and simulated using CST Studio based on the requirements from chapter 2 and the parameters of the Xethru X4. Then a simplified version of the radar system is modeled in Matlab. This model contains parameters and variables from the radar, the target and the environment.

5.1. Antenna

Since the radar system model in this chapter is based on the Xethru X4, the antenna will also be designed to match this radar system. Using the X4 datasheet and the requirements from chapter 2 a list of design specifications for the antenna can be derived [12]:

- The transmitter and receiver will share the same antenna design.

- The antenna design takes complexity and production costs into account.

- The antenna must have a bandwidth (S_{11} < -10dB) of at least 2.5 times the bandwidth of the main lobe of the transmitted signal ($2.5/\tau$) to capture more signal energy and preserve more fidelity of the transmitted signal [20]. The bandwidth should range from at least 5.5 - 9.1GHz.

- The antenna must have a broad radiation pattern to be able to detect target at many angles.

- Both antennas will be located close to each other, the radiation pattern must feature blind spots such that the antennas can be strategically positioned to prevent spillover.

Using these design specifications a patch antenna was designed and simulated in CST Studio. An UWB patch antenna design found in literature was used as a reference starting point [18]. This design deploys three methods to improve the antenna bandwidth:

1. Patch steps were cut into the corners of the patch to introduce resonances at different frequencies. The steps at the corners are created when fusing differently sized patches together, each with their respective resonant frequencies.

2. A partial ground plane is used. This eliminates a ground plane directly behind the patch, greatly reducing the amount of energy stored in the substrate, which reduces the Q factor. By reducing the Q factor resonance is smoothed and the bandwidth increases.

3. A slot is cut in the patch introducing additional resonant frequencies depending on the slot size.

5.1.1. UWB Patch Antenna

The simulated antenna is a patch antenna on an FR-4 substrate with a partial ground plane. FR-4 is a class of materials with an average relative permittivity ϵ_r of 4.4 that is used as a base for PCB's. The substrate is modeled using lossy FR-4 and the metal layers are modeled as perfect electric conductors (PEC) to reduce simulation time. PEC modeling is common when simulating antennas since metallic losses are relatively low [18]. The antenna design is shown in figure 5.1.
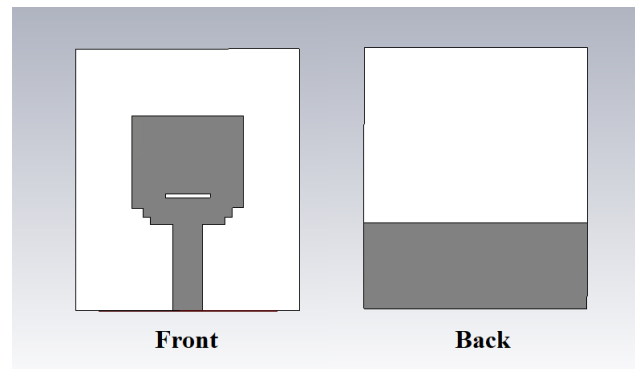
Figure 5.1: Design of the antenna: front view showing the patch, back view showing the partial ground plane.

5.1.2. Dimensions

Determining the dimensions of the patch, the steps, the ground plane and the slot is difficult mathematically. There are many factors at play that change the resonant frequencies of the patch. Theoretically, a patch antenna works similar to a halfwave dipole, and is thus about half a wavelength long. In reality this is not exactly the case. Because the antenna is built on a dielectric substrate, the electric fields induced by the antenna feed are fringed at the patch's outside edges, which increases the effective size. This phenomenon makes patch antenna's smaller than their dipole counterpart. Determining the optimal dimensions for the patch is best achieved using several simulation iterations while making small adjustments. The design from [18] was used as a base design. The antenna was implemented as a parametric model, allowing easy adjustment of dimensions. After several iterations, the best results were achieved using the following dimensions:

- The substrate measures 30 x 35 mm and is 1.6 mm thick.

- All metal layers are 0.035 mm thick.

- The ground plane measures 30 x 11.5 mm.

- The feed line measures 4 x 11.5 mm.

- The patch measures 14.5 x 15 mm.

- The bottom step measures 1 x 1 mm.

- the second step measures 1.5 x 1.2 mm.

- the slot measures 6 x 0.5 mm and is positioned at 3.6 mm distance from the end of the feed line.

5.1.3. Bandwidth

The bandwidth of the antenna is determined by measuring the return loss as a function of frequency. At resonant frequencies the return loss is expected to be below -10dB, thus by using the three techniques described in section 5.1 a high bandwidth is expected. Using CST, after 8 iterations, the return loss was simulated from 0 to 15 GHz. The S-parameter evaluation was done using a normalized impedance of 50Ω, this corresponds to the impedance of the antenna terminals on the Xethru X4 chip [12]. The result is shown in figure 5.2.

Figure 5.2 shows that the bandwidth of the antenna is about 3.2 - 14 GHz by looking where the curve crosses the -10dB points. This ensures all the signal bandwidth can be transmitted and received with full fidelity.

5.1.4. Radiation Pattern

The radiation pattern of the antenna has been simulated in 3d using CST. The pattern is donut shaped with dead spots along the axis of the feed line. A visual representation is given in figure 5.3.

The polar plots of the radiation pattern rotating along the X-axis shown in figure 5.3 are given in figure 5.4.
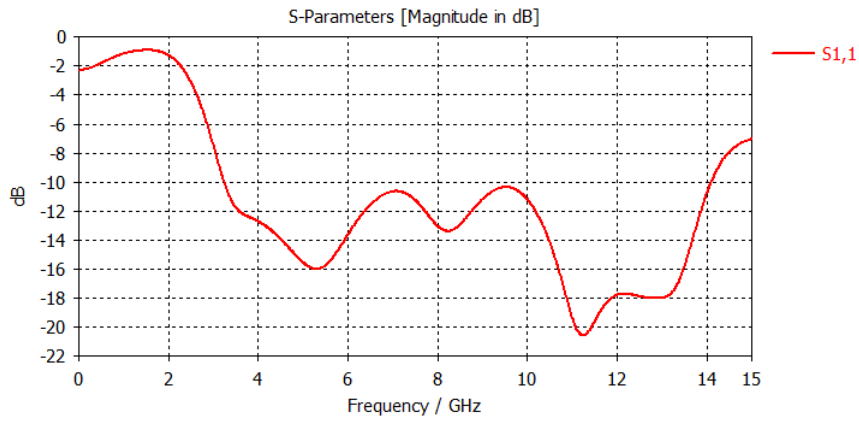
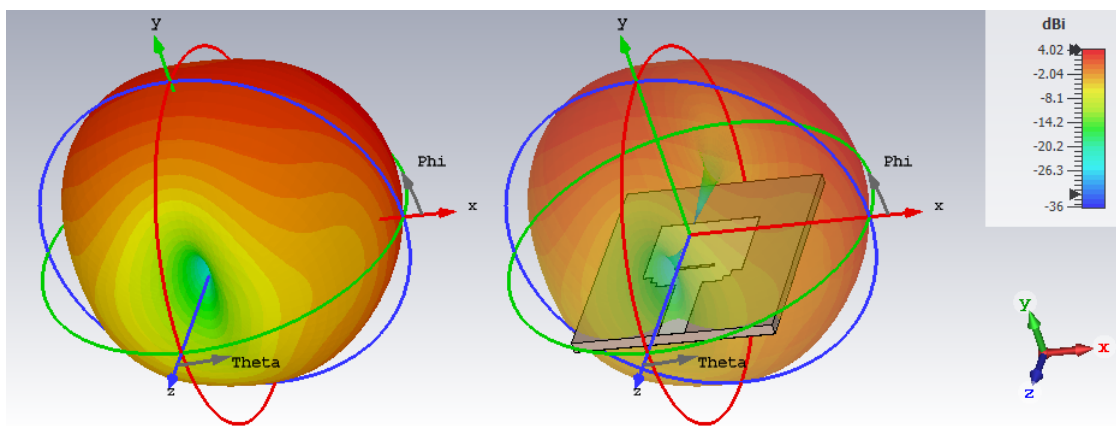Figure 5.2: Return loss in dB as a function of frequency in GHz

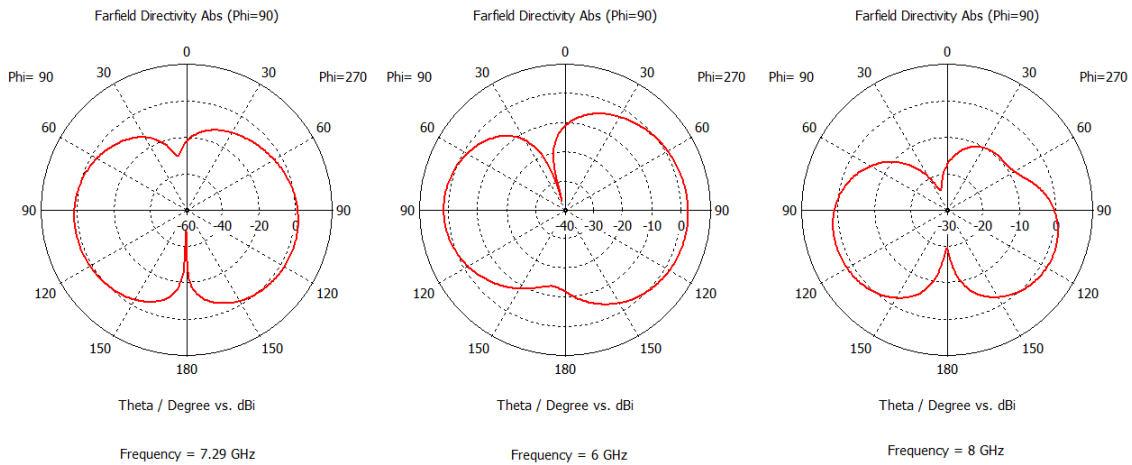Figure 5.3: 3d plot of the radiation pattern at 7.29GHz

Figure 5.4: Polar plot at 7.29GHz, 6GHz and 8GHz

The radiation pattern varies depending on the input frequency as is shown in figure 5.4. The pattern remains donut shaped along all the frequencies in the Xethru X4 signal bandwidth. This pattern can be exploited when placing the transmitter and receiver to greatly reduce radiation spillover, see section 5.1.5.

5.1.5. Antenna Configuration

The configuration of the transmitter and receiver antennas have to comply to the requirements from section 2. The requirements state that the radar system should be a single device. This means the transmitter and receiver will be located in close proximity to each other. As was mentioned in section 5.1.4 the antenna features dead spots at the feedline and the tip of the patch. By placing the antennas with these dead spots facing each other, along the direct line of sight path, the spillover interference is greatly reduced. Figure 5.5 shows a proposed configuration on a PCB in which the antennas are oriented in the same polarization while minimizing the direct interference to the receiver.
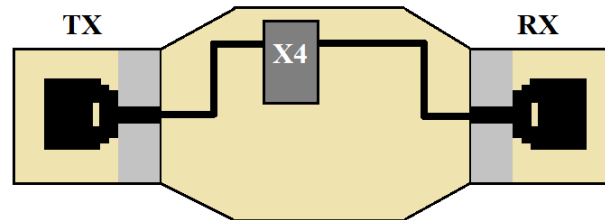

Figure 5.5: Proposed antenna configuration on a 1.6 mm FR-4 PCB

5.1.6. Tolerances

When producing an antenna from a simulated design, it can not be expected to be a perfect reproduction. Errors in the dimensions can occur, as well as inconsistencies in the dielectric substrate. FR-4 is a class of PCB material. The simulated dielectric constant ϵ_r is 4.4 but depending on the manufacturer of the PCB antenna, this can be higher or lower. This inconsistency is mostly caused by variance in the ratio of resin and glass fibre. It can be expected that the distribution of resin versus glass fibre is not uniform throughout the PCB. FR-4 will also show different values for ϵ_r depending on the frequency that was used to measure it [25]. The reason FR-4 was chosen regardless of these issues is that it is very cheap compared to more advanced materials such as RO4003 laminate by Rogers Corporation. The antenna bandwidth was chosen to be large deliberately to accommodate for any loss in bandwidth that might occur due to production errors and material inconsistencies.

5.2. Target model

The target model includes information about the possible ranges that the target can have, the chest movement due to respiration and the radar cross section. Chest movement caused by heartbeat is much smaller in comparison and not necessarily required for human detection. This model will not include heartbeat motion.

5.2.1. Respiration model

Respiratory motion in humans can be seen as expansion and retraction of the chest. This causes movements in many directions but motion is most prominent, about 2cm, along the anteroposterior axis [11]. To simplify this problem, the motion is modelled as a moving target with a static shape. The motion is modelled as a sine wave with an 8mm amplitude and 0.25Hz frequency. The amplitude is less than 2cm because motion along the anteroposterior axis also includes motion at the back, which is excluded in the model. Additionally a conservative estimate should be made relative to the value found in literature since the system will be used to detect young children instead of adults.

5.2.2. Radar cross section

Radar cross section (RCS) measures the ability to detect a target. The ability of a target to reflect the incident signal back is dependent on many different factors. Many targets in radar applications have very complex surfaces with different materials. This makes it very difficult to determine the RCS mathematically. RCS is expressed as the surface area of a perfectly conducting spherical target, in m^2. This means that assigning a value of RCS to a target essentially models it as a perfectly conducting sphere with a certain area.

To model the RCS of a human chest, two approaches were considered:

- Model the chest as a perfect electric conducting ellipsoid with dimensions similar to the chest of a young child. For this approach an approximation for the RCS was found in literature [26]. The RCS changes depending on incident angles and size of the ellipsoid. The size, determined by the radius of the ellipsoid along all 3 axis are expressed by a, b and c, the incident angle is expressed by the azimuth angle θ and the elevation angle ϕ. σ is the RCS, see formula 5.1.

$$\sigma = \frac{\pi a^2 b^2 c^2}{(a^2(sin\phi)^2(cos\theta)^2 + b^2(sin\phi)^2(sin\theta)^2 + c^2(cos\phi)^2)^2} \quad (5.1)$$

Using this formula with approximated dimensions for a baby's chest, an RCS of 0.01 m^2 was found. This means that the baby is modelled as a PEC sphere with area 0.01 m^2 which seems very small.

- Model the chest with a static RCS from all angles using an RCS value based on a measurement. In literature it was found that RCS of a human target is highly variable but for adults is about 1 m^2 on average [27]. As a conservative estimate, an RCS of 0.5 m^2 was used in the simulations.

The model of an ellipsoid seems to give RCS values that are very low in comparison with the average measured RCS found in literature. Although, further inspection in literature reveals that RCS can be very low depending on posture. To stress test the radar system, the low RCS from the ellipsoid model will be used as well.

5.2.3. Target range
One of the user requirements is to have a coverage over the entirety of the car. The model considers three possible positions which are defined as follows:

- position 1: the target is in the middle of the back seat of the car.

- position 2: the target is next to the window of the back seat of the car.

- position 3: the target is in the front seat of the car.

The distance from the radar to these positions were estimated based on the radar being placed at the center of the roof, as can be seen in figure 5.6.
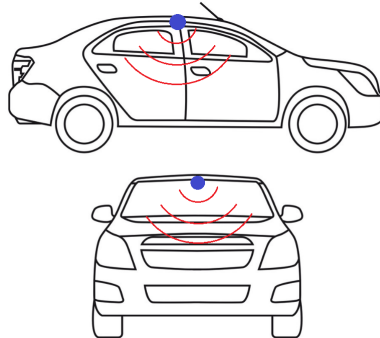

Figure 5.6: Placement of the radar as a reference for simulations.

The position coordinates are added to the sinusoidal motion such that the model becomes a sinusoidal motion that is changing between $+/- R_{resp}$ at position (x,y,z). Figure 5.7 shows the described motion.

The range is calculated in MATLAB. The code is given in appendix B.2. The results are shown in table 5.1. The obtained values are consistent with the implications of changing the range. The received power of position 1 and 3 are almost equal. This is due to the increased cone angle which reduced the advantage of having the target close to the radar. The received power and the SNR are reduced according to the range. The radar cross section remains relatively unchanged. This is explained in section 5.2.2.
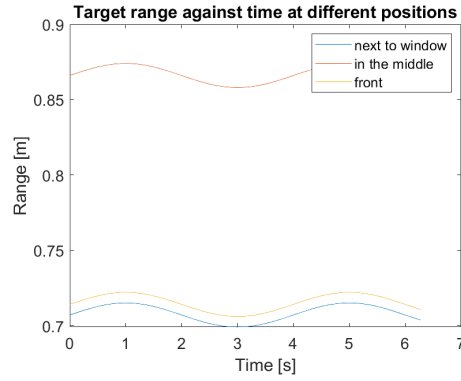
Figure 5.7: The range of the target at different positions.

	Position 1	Position 2	Position 3
$(x, y, z)[m]$	$(0.5, 0, -0.5)$	$(0.5, 0.5, -0.5)$	$(0.1, 0.5, -0.5)$
$(\theta, \phi)[deg]$	$(0, -45)$	$(45, -45)$	$(45, -35.3)$
$R_{max}[m]$	0.715	0.874	0.722
$RCS[m^2]$	0.0139	0.0099	0.0136
$P_r[dB]$	-79.6	-84.6	-79.9
SNR	19.65	14.67	19.37

Table 5.1: Implications on radar parameters at different target positions assuming $L_s = 1dB$. θ corresponds to the azimuth and ϕ is the elevation as seen from the radar.

5.3. Channel and environment

The wave propagation in the car is subjected to free space loss. Furthermore, increased temperature is taken into account. The estimated SNR using equation 4.8 is calculated for different temperatures. The calculation is done with system losses of $L = 1dB$, range of $R = 0.87m$ and $RCS = 0.01m^2$.

$$SNR(T = 290) = 14.67 \qquad \text{[dB]} \quad (5.2)$$

$$SNR(T = 323) = 14.2 \qquad \text{[dB]} \quad (5.3)$$

The maximum change in SNR due to temperature is around $0.5dB$, which is a reasonable value since the SNR is already high. In conclusion, increasing the temperature up to 50 degrees Celsius will not compromise the system performance significantly. Therefore, in terms of temperature tolerance, Xethru performs well.

5.4. Radar equation

The received power at different transmitted peak powers is shown in 5.8. The chosen transmit peak powers correspond to the possible peak powers of Xethru. The noise power which is calculated using equation 4.7 to be $-100dB$, is also shown in the figure. The intersection of the received power with the noise indicates the maximum range at which reflections are reliably detected with the given transmitted peak power.

The minimum required SNR is assumed to be $3dB$ which implies that the received power should be at least double the noise power. The maximum range values are given in table 5.2.

The received power at different radar cross sections is shown in figure 5.9. The horizontal line at $-100dB$ corresponds to the noise power and the other horizontal line corresponds to the received power at $RCS = 0.5m^2$. The calculations are done with the highest peak power setting and assuming the target is in position 2 which has a range of $R = 0.87m$.

The RCS based on the ellipsoid model is very small, only $0.01m^2$, which yields low received power and consequently lower SNR as can be seen in figure 5.9. Using the assumption that the RCS of children is about $0.5m^2$ yields a gain in received power of about $17dB$.
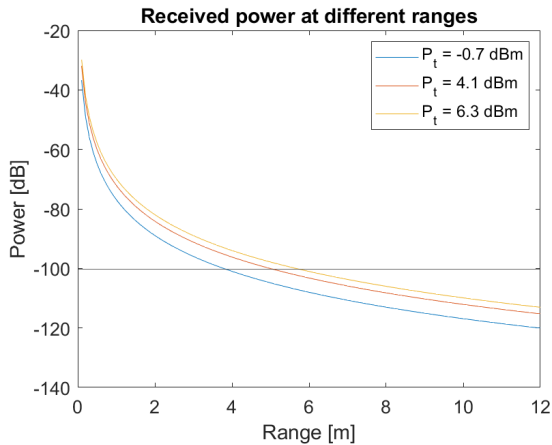
Figure 5.8: Received power at different ranges with noise power of $-100dB$ with $RCS = 0.5$ and target range of $0.87m$.
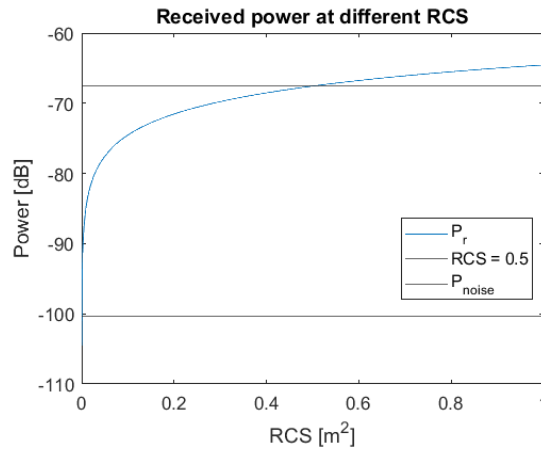

Figure 5.9: Received power at different RCS. Selected RCS of 0.5 is plotted. The noise power specified as $-100dB$. The transmit peak power is $6.3dBm$ and the target range is $0.87m$.

$P_{peak}[dBm]$	$R_{max}[m]$
-0.7	3
4.1	4
6.3	4.5

Table 5.2: Maximum range (SNR > 3dB) for all transmit power settings, RCS = 0.5 m^2.

5.5. Threshold detection

When using threshold detection, the parameters of interest are the SNR, probability of detection P_D and the probability of false alarm P_{fa}. The relation between those parameters can be visualized using receiver operating characteristic plots. This plot is applicable for coherent receivers with nonfluctuating target [28]. The fluctuations in this context is described as changes in the radar cross section [29]. Since this is not the case as has been shown in table 5.1, the plot is still applicable for the case at hand.

The SNR is estimated at position 2, at which the range is $R = 0.87[m]$, radar cross section of $RCS = 0.01[m^2]$ and transmitted peak power of $6.3[dBm]$. The probabilities are shown in figure 5.10. For the given SNR, threshold detection can be reliably applied for range detection since P_D is high and P_{fa} is very low, due to the high SNR. For the given application, false alarms that occur frequently can lead to the user to neglect the alarm and consequently, children can be left in the car which is the essential problem that the radar should solve.
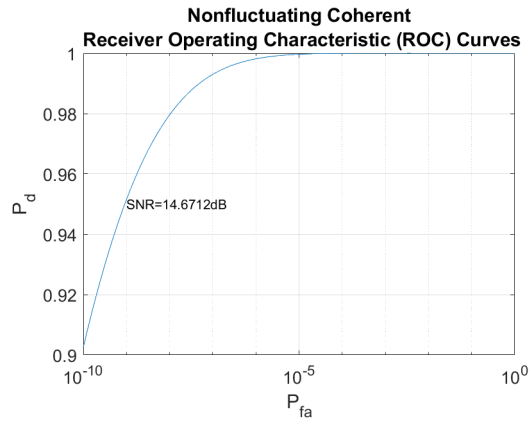
Figure 5.10: ROC at the estimated SNR at range
$R = 0.87[m]$.

5.6. Doppler detection

The Doppler shift as a function of time is shown for different cone angles corresponding to the possible positions. Formula 3.1 shows the dependence on the cone angle of the target. This is demonstrated in figure 5.11.

The formula also shows the dependence on the carrier frequency. This is shown in figure 5.12 as the Doppler shift increases with the carrier frequency. Since the clutter is always concentrated around 0 Hz, it is required to have higher Doppler shifts i.e. higher carrier frequencies. The limitations are regulations, costs and technology. Implementing a patch antenna with very high frequency increases the losses and makes it more susceptible to fabrication errors. This can be solved using more expensive materials and production methods. As for the regulations for indoor UWB technology, if the maximum allowed emission levels are to be used, the upper bandwidth must not exceed 10.6 GHz.

As the figure shows, the carrier frequency of Xethru can lead to a maximum Doppler shift of about $0.5Hz$. At this frequency and with the presence of phase noise, the clutter can be close to this frequency. This means that measuring Doppler shift with Xethru requires non-trivial signal processing algorithms to distinguish the Doppler shift from the clutter.
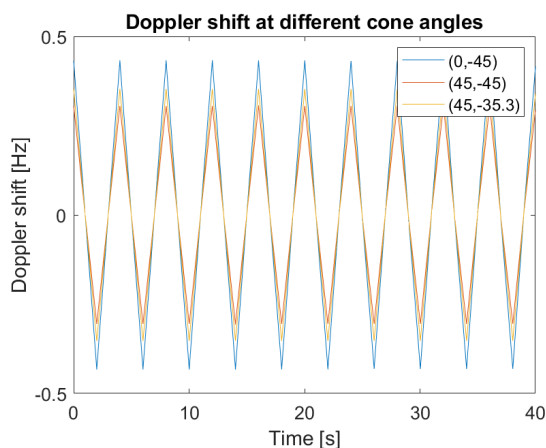

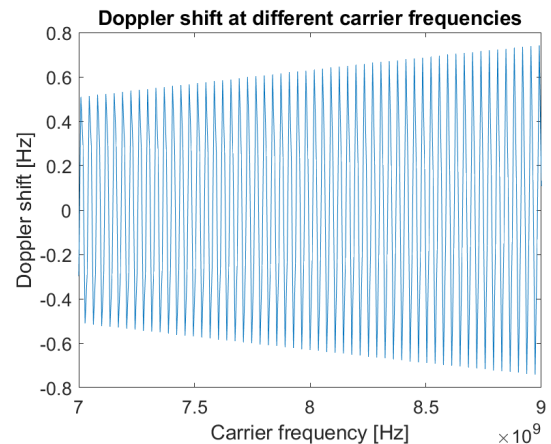Figure 5.11: Doppler shift at different azimuth angles

Figure 5.12: Doppler shift at different carrier frequencies assuming $cos(\theta_{cone}) = 1$

<div style="text-align: right; font-size: 4em;">6</div>

Discussion

6.1. Assumptions and Simplifications

Field testing was not possible within the project's time frame so the model is based purely on theory, simulations and previous research. To make this model a feasible approach, some assumptions and simplifications were made. These are discussed in this chapter.

6.1.1. Radar Equation Model

The radar equation models the significant parameters of a radar, however, there are loss mechanisms that are not considered in the calculations. It is assumed that the system losses $L = 1dB$. However, the losses depend on the total system such as signal processing losses, atmospheric losses, transmit and receive losses (losses between transmitter/receiver and antenna) .. etc. This should be taken into account by practically estimating this value.

Additionally, the system is subject to large amounts of multipath propagation. The Xethru X4 is able to take advantage of this with a high range resolution. The received power can be greatly increased when receiving multiple paths, however this power gain has not been modeled since it was too complex to estimate. Despite this the radar still showed to be able to detect target at ranges that are expected in a car environment.

Furthermore, the maximum range at a certain peak power can be different due to the radar cross section. A study on human RCS showed that the reflectivity of the human body is highly dependant on posture. If a baby inside a car is positioned such that the RCS is minimal, the radar will have a reduced max range for detection.

6.1.2. Respiration Model

The target respiration model assumes that the chest motion due to respiration is sinusoidal. However, the actual movement is different. The chest movement can have many frequency components such that an accurate model would take those into consideration as well. By means of spectral analysis, each frequency can be analyzed [7].

6.1.3. Target Model

RCS has shown to be highly variable. An attempt was made to model the target as an ellipsoid. Using this model a mathematical expression for the RCS was possible [26]. The model resulted in RCS values much lower than reported in literature [27]. Ideally, the RCS would be measured. The RCS can be estimated using the radar equation, because the transmitted power, the received power and the range are known. This estimation is subject to inaccuracy because of losses and multipath gain that is factored into the radar equation. Alternatively, using a reference target with known RCS, the system could be calibrated for more accuracy on infant RCS measurements.

6.1.4. Radar Placement

In the system model the radar was placed at the center of the car's roof. This allowed for close proximity to targets on all seats. An issue that could occur with this placement is the the passengers located in

the front of the car will have their chest moving largely perpendicular to the radial axis of the radar. This can potentially make it hard to detect vital signs. Alternatively, the radar can be placed near the front of the car at the rear view mirror. In this configuration the radar is aimed better in the direction of the chest motion for all passengers. A downside is the increased distance to the backseats where children are commonly situated, this degrades the SNR. Additionally, a child sitting in the front passenger seat can potentially block the direct line-of-sight path to a child in the backseat.

6.1.5. Doppler Shift Measurement

For the detection of small Doppler shift, the phase noise should be minimized such that the clutter spectrum is as close as possible to 0 Hz. However, if during measurement, a movement occurs with a speed that is relatively larger than the movement of interest, then the larger motion will dominate and the the smaller Doppler shift will become hard to detect. An example to that is random body movement. For the given context, if the infant moves a hand or a leg, then this motion can be seen as noise. Many techniques have been employed to cancel for random body movement such as phase compensation where the induced phase of the RBM is measured using a camera and then this value is subtracted from the phase of the received signal [30, 31].

6.1.6. SNR Estimation

To estimate the SNR, the system noise has to be modeled. In the model used for the simulation, the noise was modeled as a flat level based on noise figure parameters from the Xethru X4 datasheet [12]. In practice, this noise is random over time. Additionally, the receiver picks up electromagnetic noise from the environment. For example, a car's electronics will generate EM noise that can degrade the SNR of the radar system. This has not been taken into account in the model. Consequently, the probabilities of detection and false alarm can be different in an actual scenario.

The calculated SNR does not account for the coherent integration gain since this is a variable that depends on the PRF and the observation time which can be chosen for either range or Doppler shift measurement. This results in a SNR improvement of N_{pulses} for coherent integration and for noncoherent integration of less than N_{pulses}, but has a minimum of $\sqrt{N_{pulses}}$.

6.1.7. Heart Rate Detection

So far the thesis discussed only the respiration detection. Heart rate detection is more challenging since the magnitude of the motion is very small. However, the frequency is slightly larger which can lead to a larger Doppler shift. When measuring the heart rate, the accuracy of the measurement should be sufficient such that the distinction can be made between the Doppler shift of the respiration and the heart beat. Heart beat measurement has been demonstrated in previous research [7].

7

Conclusion

7.1. Summary

To prevent the deaths of babies being left in hot cars a non-contact human vital sign detection system is needed. Using the user requirements, several technologies were considered. After a state-of-the-art analysis, radar was chosen to be a suitable technology for human vital sign detection. The user requirements were used to define technical specifications relevant for a radar system.

Several radar systems were considered for the application. By means of a comparison, and considering the advantages and disadvantages in the context of the application, UWB pulsed radar was chosen to be a robust radar technique.

To test the viability of an UWB pulsed radar, the Xethru X4 System on Chip UWB Pulsed Radar was analyzed. This radar operates with a 1.4 GHz bandwidth centered around a carrier frequency of 7.29 GHz. A system analysis has been done based on the Xethru X4 parameters. Based on a theoretical analysis combined with simulations it can be concluded that an UWB pulsed radar system using Xethru X4 is suitable for detecting vital signs in a car. Table 7.1 shows the results of this analysis.

7.2. Alternatives

Xethru X4 has be shown to be a suitable radar system for vital sign detection inside a car. This does not mean that other radar techniques will not work for this application. Today there are many researchers working on radar based vital sign detection, using many techniques. Continuous Wave (CW) radar has been used as well as Frequency Modulated Continuous Wave (FMCW) to detect breathing and heart-rate frequencies [7, 9]. CW can not detect range and FMCW suffers from poor range resolution in comparison to UWB pulsed radar. Other UWB pulsed radar systems have been used to detect human vital signs in different frequency bands. For example, human presence can be detected using millimeter wave radars at frequencies of 30 GHz and higher [32]. MmWave technology suffers from high attenuation when penetrating materials, as well as requiring a license in most countries at the operating frequency bands.

Parameter	Xethru X4	Conclusion
Carrier frequency	7.29 GHz	- Allows penetration through non-metal materials revealing hidden targets. - Breathing translates to a Doppler shift of around 0.5 Hz, which can be detected when phase noise is low. - Antenna size is inversely proportional to carrier frequency, a suitable antenna was simulated with a 30x35 mm footprint.
Bandwidth	1.4 GHz	- The occupied bandwidth lies within the unlicensed spectrum for indoor UWB radar use. - The bandwidth is relatively large, allowing for 10 cm range resolution - The high range resolution is perfect for in-car applications, where multipath propagation is prominent.
Transmit power	<-9.69 dBm	- Transmit power can be set to different levels but stays below -9.9 dBm emission limits. - Signal is sent in pulses, allowing high peak power for clear detection, while maintaining low average power emissions.
Information	Digital domain	- Received signal is sampled in pass-band using swept threshold sampling for high resolution with minimal hardware. - Signal processing is done in the digital domain allowing for System on Chip design using CMOS technology.
Detection	Coherent	- Allows doppler shift to be detected - Increases SNR
Antenna	Microstrip patch	- Small antenna type that can be made on FR-4 PCB material. - Pairs well with Xethru X4 SoC which can be integrated on the same PCB.
Range	<4.5 m	- Simulations using Xethru X4 showed a maximum range of 4.5 m at the highest transmit power - The SNR stays above 3 dB within this range - For monitoring vital signs inside a car this range is more than enough to cover the inside of the car.

Table 7.1: Conclusions of system analysis on Xethru X4.

Bibliography

[1] KidsandCars.org. *Heatstroke*. URL: https://www.kidsandcars.org/how-kids-get-hurt/heat-stroke/.

[2] Jae Sim, Yonnim Lee, and Ohbyung Kwon. Acoustic sensor based recognition of human activity in everyday life for smart home services. *International Journal of Distributed Sensor Networks*, 2015:1–11, 09 2015.

[3] Xuyu Wang, Runze Huang, and Shiwen Mao. Sonarbeat: Sonar phase for breathing beat monitoring with smartphones. pages 1–2, 09 2017.

[4] T. Negishi, G. Sun, H. Liu, S. Sato, T. Matsui, and T. Kirimoto. Stable contactless sensing of vital signs using rgb-thermal image fusion system with facial tracking for infection screening. In *2018 40th Annual International Conference of the IEEE Engineering in Medicine and Biology Society (EMBC)*, pages 4371–4374, 2018.

[5] A. E. Fathy, L. Ren, S. Nahar, and O. Kilic. Overview of human vital signs detection using radar techniques. In *2017 IEEE International Symposium on Antennas and Propagation USNC/URSI National Radio Science Meeting*, pages 1229–1230, 2017.

[6] Mamady Kebe, Rida Gadhafi, Baker Mohammad, M. Sanduleanu, Hani Saleh, and Mahmoud Al-Qutayri. Human vital signs detection methods and potential using radars: A review. *Sensors*, 20:1454, 03 2020.

[7] J. Tu, T. Hwang, and J. Lin. Respiration rate measurement under 1-d body motion using single continuous-wave doppler radar vital sign detection system. *IEEE Transactions on Microwave Theory and Techniques*, 64(6):1937–1946, 2016.

[8] Gregory A. Showman. *Principles of Modern Radar*, chapter 21. An Overview of Radar Imaging.

[9] G. Wang, C. Gu, T. Inoue, and C. Li. A hybrid fmcw-interferometry radar for indoor precise positioning and versatile life activity monitoring. *IEEE Transactions on Microwave Theory and Techniques*, 62(11):2812–2822, 2014.

[10] Merrill I Skolnik. *Radar Handbook, 2nd Edition*. McGraw-Hill, 1990.

[11] J M Moll and V Wright. An objective clinical study of chest expansion. *Annals of the Rheumatic Diseases*, 31(1):1–8, 1972.

[12] Novelda. X4 datasheet ultra wide band (uwb) impulse radar transceiver soc. `https://novelda.com/x4-soc.html`, 2016.

[13] Bob Muro. *Characterizing RADAR Interference Immunity*. URL: https://boonton.com/resource-library/articles/artmid/1867/articleid/1118/characterizing-radar-interference-immunity.

[14] Y. Liu, S. Sheelavant, M. Mercuri, P. Mateman, J. Dijkhuis, W. Zomagboguelou, A. Breeschoten, S. Traferro, Y. Zhan, T. Torf, C. Bachmann, P. Harpe, and M. Babaie. 9.3 a680 μw burst-chirp uwb radar transceiver for vital signs and occupancy sensing up to 15m distance. In *2019 IEEE International Solid- State Circuits Conference - (ISSCC)*, pages 166–168, 2019.

[15] Seyed Parizi. *Bandwidth Enhancement Techniques*. 11 2017.

[16] Mohamed Salah KAROUI, Nadia Ghariani, Mongi Lahiani, and Ghariani Hamadi. A compact uwb elliptic antenna for indoor localization system. *IEICE Electronics Express*, 07 2019.

[17] A. H. M. Z. Alam, M. R. Islam, and S. Khan. Design and analysis of uwb rectangular patch antenna. In *2007 Asia-Pacific Conference on Applied Electromagnetics*, pages 1–3, 2007.

[18] Seok Choi, Jong Park, Sun Kim, and Jae Park. A new ultra-wideband antenna for uwb applications. *Microwave and Optical Technology Letters - MICROWAVE OPT TECHNOL LETT*, 40:399–401, 03 2004.

[19] Chanwoo Kim, Soonwoo Park, Heeje Han, Jaemin Bae, and Hongjoon Kim. Detection system of human respiration position using phased array antenna. *The transactions of The Korean Institute of Electrical Engineers*, 68:1002–1004, 08 2019.

[20] Mark A. Richards William A. Holm. *Principles of Modern Radar*, chapter 8. Doppler Phenomenology and Data Acquisition.

[21] Suiyan Geng, S. Ranvier, Xiongwen Zhao, J. Kivinen, and P. Vainikainen. Multipath propagation characterization of ultra-wide band indoor radio channels. In *2005 IEEE International Conference on Ultra-Wideband*, pages 11–15, 2005.

[22] Mark A. Richards. *Principles of Modern Radar*, chapter 15. Threshold Detection of Radar Targets.

[23] Byron Murray Keel. *Principles of Modern Radar*, chapter 20. Fundamentals of Pulse Compression Waveforms.

[24] Here's how hot temperatures can get in your car. `https://www.clickorlando.com/news/2019/09/26/heres-how-hot-temperatures-can-get-in-your-car`.

[25] Stephen Mumby and Jih Yuan. Dielectric properties of fr4 laminates as a function of thickness and the electrical frequency of the measurement. *Journal of Electronic Materials - J ELECTRON MATER*, 18:287–292, 03 1989.

[26] Bassem Mahafza. Radar systems analysis and design using matlab. 2nd ed. *IEEE Aerospace and Electronic Systems Magazine*, 21, 01 2000.

[27] E. Piuzzi, Stefano Pisa, Paolo D'Atanasio, and A. Zambotti. Radar cross section measurements of the human body for uwb radar applications. 05 2012.

[28] P. Swerling. Probability of detection for fluctuating targets. *IRE Transactions on Information Theory*, 6(2):269–308, 1960.

[29] James A. Scheer. *Principles of Modern Radar*, chapter 3. Radar Search and Overview of Detection in Interference.

[30] C. Gu, G. Wang, T. Inoue, and C. Li. Doppler radar vital sign detection with random body movement cancellation based on adaptive phase compensation. In *2013 IEEE MTT-S International Microwave Symposium Digest (MTT)*, pages 1–3, 2013.

[31] C. Gu, G. Wang, Y. Li, T. Inoue, and C. Li. A hybrid radar-camera sensing system with phase compensation for random body movement cancellation in doppler vital sign detection. *IEEE Transactions on Microwave Theory and Techniques*, 61(12):4678–4688, 2013.

[32] Ashish Kumar Singh and Yong Kim. Analysis of human kinetics using millimeter-wave micro-doppler radar. *Procedia Computer Science*, 84:36–40, 12 2016.

A
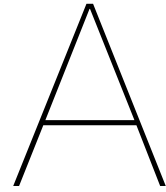
Xethru X4

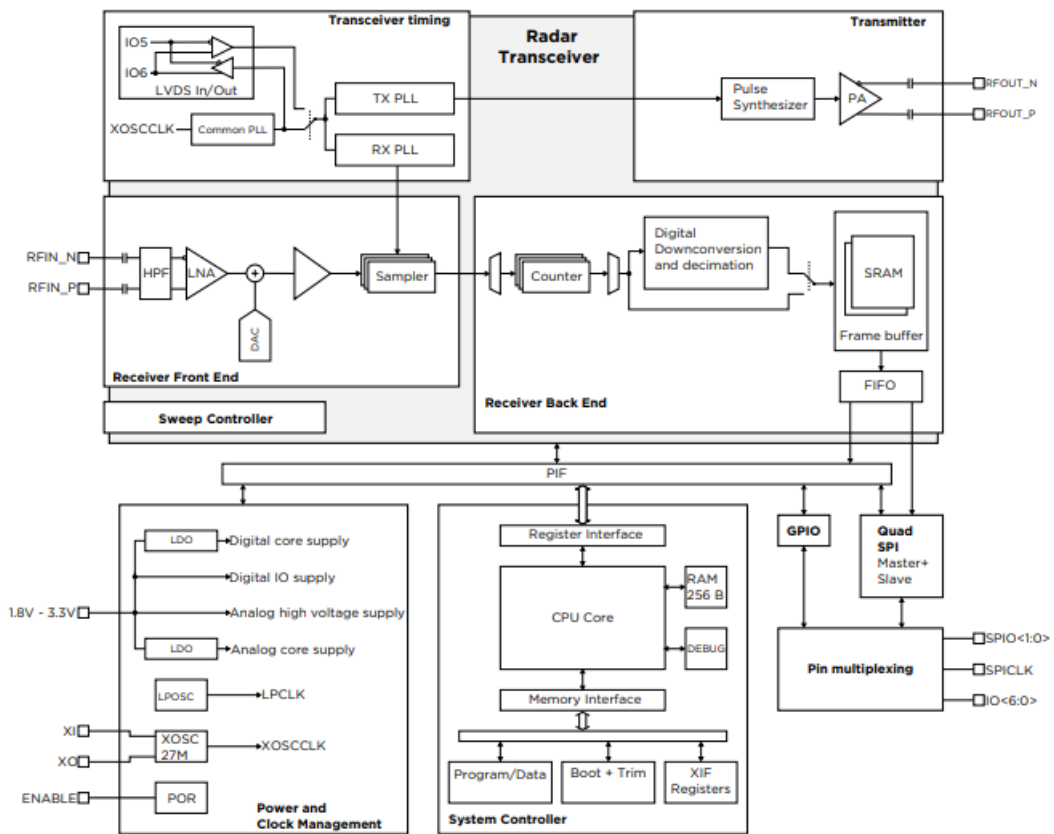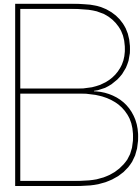The figure below shows a block diagram of the Xethru X4 radar system.

Figure A.1: Circuit overview of Xethru radar system.

B

MATLAB Code

B.1. Calculations

The calculations are done using the following code.

```matlab
1  clear all;
2  close all;
3
4  %% constants
5  c = physconst('LightSpeed');
6  k = physconst('Boltzmann');
7
8  fc = 7.29e9;                        % carrier frequency in Hz
9  lambda = c/fc;                      % wavelength in m
10 G_rx = 14.1;                        % receiver gain in dB
11 G_ant = 2;                          % antenna gain in dB
12 Ls = db2pow(1);                     % system losses of 1 dB
13
14 temp = 290;        % reference temperature in K
15 F_rx = 6.7;        % receiver noise figure
16
17 r_resp = 8e-3;     % magnitude of chest movement in m
18 f_resp = 0.25;     % frequency of chest movement in Hz
19
20 fs = 1e3;          % not to confuse it with sampling frequency
21                    % fs is used to ensure that all arrays have same length
22 bw_tx = 1.4e9;         % transmitter bandwidth
23 B = 2.5*bw_tx;         % receiver bandwidth
24
25 %% Power calculation
26 Pp_dbm = [-0.7 4.1 6.3];            % peak power in dBm
27 Pp = 10.^((Pp_dbm - 30)/10);        % peak power in W
28 Ep = 1e-12*[0.45 1.47 2.65];        % energy per pulse in J
29 pw = Ep./Pp;                        % pulse width in s
30 prf = 100;                          % pulse repitition frequency in Hz
31 Pavg = pow2db((pw*prf).*Pp)+30;     % average power in dBm
32 prf_max = 40.5e6;                   % maximum Xethru prf
33 Pavg_max = pow2db((pw*prf_max).*Pp)+30;
34
35 %% Target range and RCS
36 % position 2 is assumed since it has larger range
37 [tgtrng,tgtang,tgtrcs] = tgt_range_rcs(r_resp,f_resp,0.5,0.5,-0.5,fs);
```

35

```matlab
38
39
40  %% SNR estimation of Xethru
41  snr_est = pow2db((Pp(3)*G_rx*G_ant^2*lambda^2*tgtrcs)/...
42      ((4*pi)^3*max(tgtrng)^4*k*temp*F_rx*B*Ls));
43
44  %% SNR at different temperatures
45  snr_17 = pow2db((Pp(3)*G_rx*G_ant^2*lambda^2*tgtrcs)/...
46      ((4*pi)^3*max(tgtrng)^4*k*290*F_rx*B*Ls));
47  snr_50 = pow2db((Pp(3)*G_rx*G_ant^2*lambda^2*tgtrcs)/...
48      ((4*pi)^3*max(tgtrng)^4*k*323*F_rx*B*Ls));
49
50
51  %% Changing target's position
52  % only y is changing which corresponds to change in seat
53  [tgtrng1,tgtang1,tgtrcs1] = tgt_range_rcs(r_resp,f_resp,0.5,0,-0.5,fs);
54  [tgtrng2,tgtang2,tgtrcs2] = tgt_range_rcs(r_resp,f_resp,0.5,0.5,-0.5,fs);
55  [tgtrng3,tgtang3,tgtrcs3] = tgt_range_rcs(r_resp,f_resp,0.1,0.5,-0.5,fs);
        % front
56
57  % estimation of received power
58  Pr1 = pow2db(Pp(3)*G_rx*G_ant^2*lambda^2*tgtrcs1/...
59      ((4*pi)^3*max(tgtrng1)^4));
60  Pr2 = pow2db(Pp(3)*G_rx*G_ant^2*lambda^2*tgtrcs2/...
61      ((4*pi)^3*max(tgtrng2)^4));
62  Pr3 = pow2db(Pp(3)*G_rx*G_ant^2*lambda^2*tgtrcs3/...
63      ((4*pi)^3*max(tgtrng3)^4));
64
65
66  % estimation of SNR
67  snr1 = pow2db((Pp(3)*G_rx*G_ant^2*lambda^2*tgtrcs1)/...
68      ((4*pi)^3*max(tgtrng1)^4*k*temp*F_rx*B*Ls));
69  snr2 = pow2db((Pp(3)*G_rx*G_ant^2*lambda^2*tgtrcs2)/...
70      ((4*pi)^3*max(tgtrng2)^4*k*temp*F_rx*B*Ls));
71  snr3 = pow2db((Pp(3)*G_rx*G_ant^2*lambda^2*tgtrcs3)/...
72      ((4*pi)^3*max(tgtrng3)^4*k*temp*F_rx*B*Ls));
73
74  % normalize plot axis
75  % t = [0:(2*pi)/(fs-1):2*pi];
76  % figure;
77  % plot(t,tgtrng1);
78  % hold on;
79  % plot(t,tgtrng2);
80  % hold on;
81  % plot(t,tgtrng3);
82  % xlabel('Time [s]');
83  % ylabel('Range [m]');
84  % title('Target range against time at different positions');
85  % legend('next to window', 'in the middle', 'front');
86  % ax = gca;
87  % ax.FontSize = 13;
88  % saveas(gcf,'target range against time.png');
89
90
91
92
```

```matlab
93
94  %% Received power at different ranges and minimum SNR
95  Prn = pow2db(k*temp*F_rx*B);
96  rcs_r = 0.5;
97  range = [0.1:0.1:12];
98
99  Pt_x1 = -0.7-30; %dB
100 Pr_x1 = pow2db((db2pow(Pt_x1)*G_rx*G_ant^2*lambda^2*rcs_r)./...
101     ((4*pi)^3*range.^4));
102 Pt_x2 = 4.1-30; %dB
103 Pr_x2 = pow2db((db2pow(Pt_x2)*G_rx*G_ant^2*lambda^2*rcs_r)./...
104     ((4*pi)^3*range.^4));
105 Pt_x3 = 6.3-30; %dB
106 Pr_x3 = pow2db((db2pow(Pt_x3)*G_rx*G_ant^2*lambda^2*rcs_r)./...
107     ((4*pi)^3*range.^4));
108
109
110 snr_1 = pow2db((Pp(3)*G_rx*G_ant^2*lambda^2*rcs_r)/...
111     ((4*pi)^3*(4)^4*k*temp*F_rx*B*Ls));
112 snr_2 = pow2db((Pp(3)*G_rx*G_ant^2*lambda^2*rcs_r)/...
113     ((4*pi)^3*(5)^4*k*temp*F_rx*B*Ls));
114 snr_3 = pow2db((Pp(3)*G_rx*G_ant^2*lambda^2*rcs_r)/...
115     ((4*pi)^3*(5.7)^4*k*temp*F_rx*B*Ls));
116
117 snr_req = db2pow(3);
118 r1 = ((Pp(1)*G_rx*G_ant^2*lambda^2*rcs_r)/...
119     ((4*pi)^3*(snr_req)*k*temp*F_rx*B*Ls))^(1/4);
120 r2 = ((Pp(2)*G_rx*G_ant^2*lambda^2*rcs_r)/...
121     ((4*pi)^3*(snr_req)*k*temp*F_rx*B*Ls))^(1/4);
122 r3 = ((Pp(3)*G_rx*G_ant^2*lambda^2*rcs_r)/...
123     ((4*pi)^3*(snr_req)*k*temp*F_rx*B*Ls))^(1/4);
124
125
126 % figure;
127 % plot(range,Pr_x1);
128 % hold on;
129 % plot(range,Pr_x2);
130 % hold on;
131 % plot(range,Pr_x3);
132 % yline(Prn);
133 % xlabel('Range [m]');
134 % ylabel('Power [dB]');
135 % title('Received power at different ranges');
136 % legend('P_t = -0.7 dBm','P_t = 4.1 dBm','P_t = 6.3 dBm');
137 % ax = gca;
138 % ax.FontSize = 13;
139
140
141 %% received power against RCS
142 rcs = [0.0001:0.001:1];
143 Pr_rcs = pow2db(Pp(3)*G_rx*G_ant^2*lambda^2*rcs/...
144     ((4*pi)^3*max(tgtrng2)^4));
145
146 Pr_rcs_half = pow2db(Pp(3)*G_rx*G_ant^2*lambda^2*0.5/...
147     ((4*pi)^3*max(tgtrng2)^4));
148
```

```matlab
149  % figure;
150  % plot(rcs,Pr_rcs);
151  % hold on;
152  % yline(Pr_rcs_half);
153  % hold on;
154  % yline(Prn);
155  % xlabel('RCS [m^2]');
156  % ylabel('Power [dB]');
157  % title('Received power at different RCS');
158  % legend('P_r','RCS = 0.5','P_{noise}');
159  % ax = gca;
160  % ax.FontSize = 13;
161
162
163  %% ROC
164  % estimated SNR
165  [pd_est,pfa_est] = rocsnr(snr_est,'SignalType','NonfluctuatingCoherent');
166
167  % figure;
168  % rocsnr(snr_est,'SignalType','NonfluctuatingCoherent');
169  % ax = gca;
170  % ax.FontSize = 13;
171
172
173  % minimum required SNR
174  snr_min = [snr_1;snr_2;snr_3];
175  [pd_min,pfa_min] = rocsnr(snr_min,'SignalType','NonfluctuatingCoherent');
176
177  % figure;
178  % rocsnr(snr_min,'SignalType','NonfluctuatingCoherent');
179  % ax = gca;
180  % ax.FontSize = 13;
181
182  %% Doppler at different positions
183  t = [0:fs/(fs-1):fs];
184  v_t = r_resp*(2*pi*f_resp)*cos(2*pi*f_resp.*t);
185
186  f_dop1 = (2/lambda).*v_t.*cos(deg2rad(0)).*cos(deg2rad(-45)); % middle
187  f_dop2 = (2/lambda).*v_t.*cos(deg2rad(45)).*cos(deg2rad(-45)); % window
188  f_dop3 = (2/lambda).*v_t.*cos(deg2rad(45)).*cos(deg2rad(-35.264)); % front
189
190
191  % figure;
192  % plot(t,f_dop1);
193  % hold on;
194  % plot(t,f_dop2);
195  % hold on;
196  % plot(t,f_dop3);
197  % xlim([0 40])
198  % xlabel('Time [s]');
199  % ylabel('Doppler shift [Hz]');
200  % title('Doppler shift at different cone angles');
201  % legend('(0,-45)','(45,-45)','(45,-35.3)');
202  % ax = gca;
203  % ax.FontSize = 13;
204
```

```matlab
205
206 %% Doppler at different carrier frequency
207 fc = [1e9:(10e9-1e9)/(fs-1):10e9];
208 f_dopc = (2/c).*v_t.*fc;
209
210 % figure;
211 % plot(fc,f_dopc);
212 % xlim([7e9 9e9])
213 % xlabel('Carrier frequency [Hz]');
214 % ylabel('Doppler shift [Hz]');
215 % title('Doppler shift at different carrier frequencies');
216 % ax = gca;
217 % ax.FontSize = 13;
```

B.2. Range and RCS calculations

Function that calculates the target range, azimuth, elevation and radar cross section.

```matlab
1  function [tgtrng,tgtang,tgtrcs] = tgt_range_rcs(r,f,x,y,z,fs)
2  % theta azimuth in rad
3  % phi elevation in rad
4  % x,y,z of target with radar being at [0;0;0]
5  % r: magnitude of respiration or heart beat
6
7  % calculate azimuth and elevation of target in (x,y,z)
8  [theta,phi,~] = cart2sph(x,y,z);
9
10 % return the cartesian coordinates of respiration
11 [xp,yp,zp] = sph2cart(theta,phi,r);
12
13 % calculate sinusoidal motion with fs samples
14 t = [0:(2*pi)/(fs-1):(2*pi)];
15
16 % apply sinusoid to the respiration xyz
17 % and add the xyz of the position
18 tgtpos = (sin(2*pi*f.*t).*[xp;yp;zp])+[x;y;z];
19
20 % calcuate range and angle tgtang=[azimuth;elevation]
21 [tgtrng,tgtang] = rangeangle(tgtpos);
22
23 % calcuate the rcs based on ellipsoid model
24 ea = 0.08;          %ea2 = thickness of the baby's torso
25 eb = 0.08;          %eb2 = width of the baby's torso
26 ec = 0.15;          %ec2 = hight of the baby's torso
27 tgtrcs = (pi*ea^2*eb^2*ec^2)/((ea^2*sin(phi)^2*cos(theta)^2)+...
28     (eb^2*sin(phi)^2*sin(theta)^2)+(ec^2*cos(phi)^2))^2;
29
30 end
```